Geomechanics and Engineering, *Vol. 37, No. 6 (2024) 599-614*
https://doi.org/10.12989/gae.2024.37.6.599

Theoretical analysis of erosion degradation and safety assessment of submarine shield tunnel segment based on ion erosion

Xiaohan Zhou[1,2], Yangyang Yang[1,2], Zhongping Yang[*1,2],
Sijin Liu[**3], Hao Wang[1,2] and Weifeng Zhou[1,2]

[1]*School of Civil Engineering, Chongqing University, Chongqing 400045, China*
[2]*National Joint Engineering Research Center of Geohazards Prevention in The Reservoir Areas (Chongqing), Chongqing 400045, China*
[3]*China Railway 14th Bureau Group Co., Ltd. Ji'nan 250014, China*

(*Received December 29, 2023, Revised June 1, 2024, Accepted June 4, 2024*)

Abstract. To evaluate the safety status of deteriorated segments in a submarine shield tunnel during its service life, a seepage model was established based on a cross-sea shield tunnel project. This model was used to study the migration patterns of erosive ions within the shield segments. Based on these laws, the degree of deterioration of the segments was determined. Using the derived analytical solution, the internal forces within the segments were calculated. Lastly, by applying the formula for calculating safety factors, the variation trends in the safety factors of segments with different degrees of deterioration were obtained. The findings demonstrate that corrosive seawater presents the evolution characteristics of continuous seepage from the outside to the inside of the tunnel. The nearby seepage field shows locally concentrated characteristics when there is leakage at the joint, which causes the seepage field's depth and scope to significantly increase. The chlorine ion content decreases gradually with the increase of the distance from the outer surface of the tunnel. The penetration of erosion ions in the segment is facilitated by the presence of water pressure. The ion content of the entire ring segment lining structure is related in the following order: vault < haunch < springing. The difference in the segment's rate of increase in chlorine ion content decreases as service time increases. Based on the analytical solution calculation, the segment's safety factor drops more when the joint leaks than when its intact, and the change rate between the two states exhibits a general downward trend. The safety factor shows a similar change rule at different water depths and continuously decreases at the same segment position as the water depth increases. The three phases of "sudden drop-rise-stability" are represented by a "spoon-shaped" change rule on the safety factor's change curve. The issue of the poor applicability of indicators in earlier studies is resolved by the analytical solution, which only requires determining the loss degree of the segment lining's effective bearing thickness to calculate the safety factor of any cross-section of the shield tunnel. The analytical solution's computation results, however, have some safety margins and are cautious. The process of establishing the evaluation model indicates that the secondary lining made of molded concrete can also have its safety status assessed using the analytical solution. It is very important for the safe operation of the tunnel and the safety of people's property and has a wide range of applications.

Keywords: analysis of seepage model; analytical solution of elastic foundation beam model; deterioration of segment; migration law of ions; subsea shield tunnel; tunnel safety analysis

1. Introduction

There will be leakage issues when the submarine structure tunnel is operating because of the multi-seam nature of the shield tunnel itself, the long-term action of water pressure, and other factors (Zhuang *et al.* 2022). Due to the increasing operational time of shield tunnels, the area of water leakage at the joints of tunnel segments is continuously expanding (Liu *et al.* 2024, Zhou *et al.* 2021). As a result, the lengthy period of operation and maintenance has progressively replaced the large-scale tunnel building phase. The composition of erosion ions in the marine environment is complex. When seawater intrusion causes ions such as sulfate, chloride, and others to erode the shield segment, segment joints deteriorate. (Qiu *et al.* 2019, Liu *et al.* 2022). The overall bearing capacity of the tunnel will inevitably decrease, threatening the safety of the tunnel operation.

Studies on the erosion and diffusion of chloride ions have been conducted recently. It is considered that the diffusion of chloride ions under the action of concentration gradient is a transmission problem in porous media (Feng *et al.* 2021). The permeability of concrete materials is a key factor affecting the migration of chloride ions (Dong *et al.* 2024). Fick's law of diffusion and Darcy's law of permeability serve as the foundation for the erosion ion transport model, which is then adjusted based on the environmental conditions. The transport analysis model of erosion ions such as chloride has gradually developed from single-factor variables to multi-factor variables. Scholars have studied the solute transport mechanism from different

*Corresponding author, Professor
E-mail: yang-zhp@163.com
**Corresponding author, Ph.D.
E-mail: 1426486908@qq.com

ISSN: 2005-307X (Print), 2092-6219 (Online)

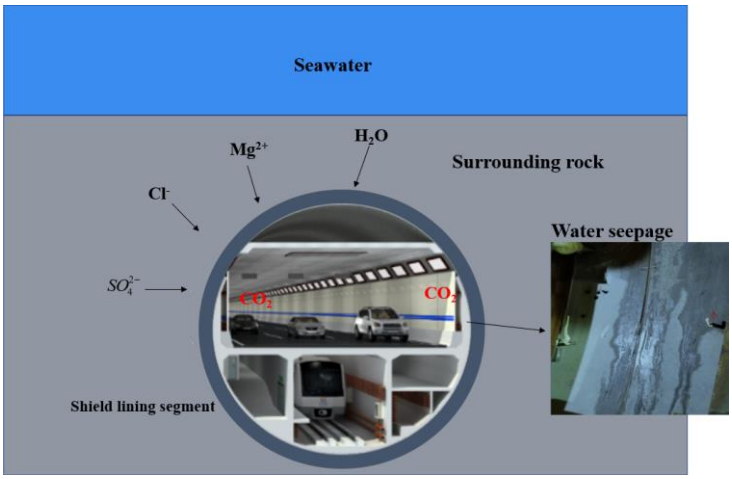

Fig. 1 Corrosion environment of submarine shield tunnel and water leakage of segment

angles (Song *et al.* 2018). The mathematical model of solute transport in porous media needs to consider the effects of convection-diffusion, as well as the seepage and solute transport in porous media under water pressure (Batany *et al.* 2019). The coupling effect of chloride ion quality, water pressure and erosion time has an impact on the diffusion coefficient (Lei *et al.* 2015). The tunnel lining structure is vulnerable to the long-term action of erosive ions, which weakens the lining stiffness (Guo *et al.* 2021), causes large deformation, encroaches on the driving space, and may even result in collapse due to lining structure fracture, endangering driving safety. At the same time, the shield tunnel itself has the characteristics of multi-slit and porous. It is easy to form a seepage channel inside the structure, which will accelerate the corrosion of ions to the segment, accelerate the loss of effective bearing thickness of the segment, and reduce the safety of tunnel operation (He *et al.* 2023).

The assessment of the safety status of the deteriorating sections of the submarine shield tunnel during its service life has been thoroughly explored by both domestic and international scholars. It is found that the limit analysis (Fu *et al.* 2021, Chen *et al.* 2019, Ghasemi and Nowak. 2018), numerical simulation (Vahab and Abdollah 2020, Milad *et al.* 2020, Wen *et al.* 2019) or mechanical learning (Dong *et al.* 2021, Liang *et al.* 2020) require practitioners to have professional quality or engineering experience, to accurately evaluate the state of tunnel diseases, and to reasonably assign the risk degree of various diseases. For mechanical learning, a large number of engineering cases need to be collected, and an expert database needs to be established for neural network training (Liu *et al.* 2021, Liu *et al.* 2022). On the other hand, although the above methods can quantitatively evaluate the bid evaluation, the applicability of various indicators needs to be further tested due to factors such as differences in geological conditions of tunnel projects (Kim *et al.* 2020). Based on the above content, it is necessary to propose an evaluation model that can directly quantify tunnel safety and facilitate engineering promotion.

Therefore, a cross-sea shield tunnel is chosen as the engineering object in order to solve the limitation of the evaluation method of the operation safety state of the submarine shield tunnel under the condition of segment deterioration and the poor applicability of the index. The seepage model is established by using SEEP / W software to study the migration mechanism of corrosive ions in the submarine shield segment and the diffusion law of corrosive ions in the shield segment under the condition of water leakage of the segment, in order to ascertain the effective bearing thickness loss degree of the segment. The analytical solution is derived using the elastic foundation's curved beam theory, and a numerical model is used to verify the equation. Then, the analytical solution and the calculation formula of safety factor are used to judge whether the segment is damaged. The research yielded an analytical solution that is straightforward in structure, broadly applicable, simple to program, and has a strong applicability of key indicators. The research findings play a significant guiding role in the diagnosis of tunnel safety. It has significant theoretical and application significance in order to guarantee the tunnel's safe operation and prevent the occurrence of shield tunnel safety accident.

2. The establishment of seepage numerical model of submarine shield tunnel

The chloride ion is the most prevalent type of ion in seawater's complex composition, and its diffusion through reinforced concrete structures plays a significant role in the deterioration of the shield lining's strength. Studying the migration law of corrosive ions in submarine shield tunnel segments, which are represented by chloride ions, is therefore crucial. The subsea tunnel segment's erosion environment is schematically depicted in Fig. 1. The presence of stray current speeds up the corrosion of the steel bar. Chloride ions permeate the passivation film, diffuse to the surface of the steel bar, or carbonize the concrete protective layer. Bicarbonate ions and carbon dioxide also enter the layer. Concrete corrodes due to sulfate ion, magnesium ion, microorganism, etc. deterioration.

The shield tunnel itself possesses both multi-hole and multi-slit features. Ion erosion in porous media is primarily

caused by pore water movement (Muthulingam and Rao 2015). The concentration of chloride ion in the shield tunnel beneath the complex marine environment is typically between 0.4% and 0.8%, exceeding the critical value of 0.3% for steel corrosion (Hodhod and Ahmed 2014). The erosive ions come into contact with the interior of the shield segment through convection, diffusion, mechanical dispersion, and other transmission effects when the high-pressure of the external seawater is applied. The shield segment lining's bearing capacity decreases inevitably under the long-term effects of erosive ions.

The cross-sea section of Xiamen Rail Transit Line 2 is used as the specific engineering object in order to study the erosion and degradation law of the transverse integral ring structure of the shield tunnel. The erosion and degradation mechanism of the entire ring segment lining of the shield segment of the subsea tunnel in the unsaturated state is studied using the numerical model of ion erosion convection-diffusion coupling theory.

2.1 Engineering situation

2.1.1 project overview

The Xiamen Rail Transit Line 2's cross-sea tunnel is being built using a shield method in conjunction with mining method. Slurry balance shield made of composite is used to construct the shield section. There are roughly 260 meters in the mine section and about 2500 meters overall. This subway tunnel is the first in China to use a shield to cross the seabed . The seabed's stratum is undulating, with a maximum overburden thickness of roughly 60 meters, a minimum overburden thickness of about 8 meters, and a maximum water pressure of roughly 0.55 MPa.

The slurry shield interval tunnel's segment design uses a general wedge-shaped segment ring; Fig. 2 depicts the segment's cross-sectional structure. The ring segments are assembled using staggered joints, with each segment having an inner diameter of 6000 mm, an outer diameter of 6700 mm, a thickness of 350 mm, a width of 1500 mm, a wedge shape of 40 mm, and an impermeability grade of P12. Each segment follows the '3 + 2 + 1' type, which consists of 3 standard A-type, 2 adjacent B-type, and 1 capping K-type. The concrete strength grade is C55.

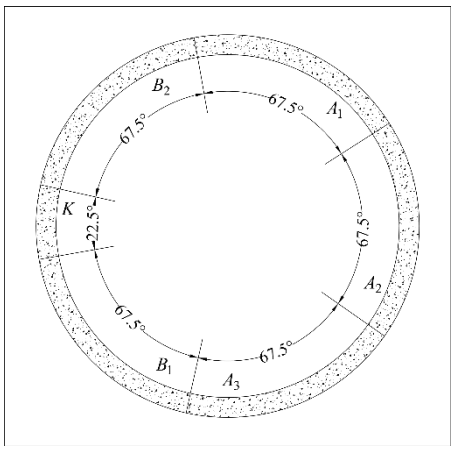

Fig. 2 Shield segment cross-section structural schematic

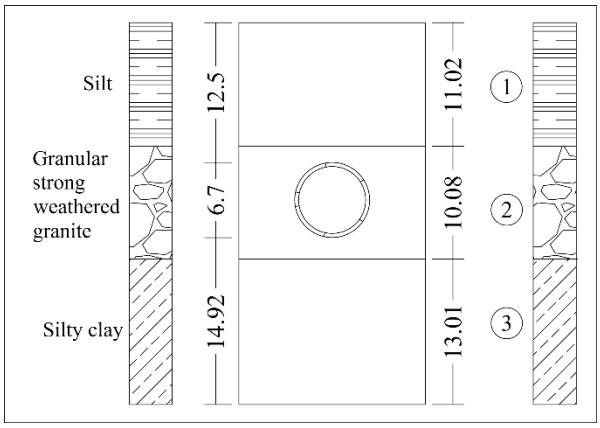

Fig. 3 Stratum distribution map (unit: mm)

2.1.2 Engineering geology

Silt, medium and coarse sand, silty clay, residual soil, a fully weathered layer, fully weathered granite, fully weathered diabase, fully weathered andesite, gabbro, a fully weathered metamorphic sandstone, a fragmented fully weathered layer, a medium weathered metamorphic sandstone, a medium weathered metamorphic quartz sandstone, a slightly weathered metamorphic quartz sandstone, and medium weathered tuff lava are among the main strata that the tunnel passes through. The sample sections are chosen for investigation based on the data from the geological exploration and the goal of the study. Figure 3 displays the stratigraphic distribution map. The geology of the construction area from top to bottom is silt, granular strongly weathered granodiorite and silty clay.

2.1.3 hydrogeology

The groundwater in the project area is mainly seawater. According to the occurrence medium of groundwater, groundwater can be divided into three categories: loose rock pore water, weathering residual pore fissure water, and bedrock fissure water Among them, the pore water of loose rock occurs in the Quaternary Holocene marine layer, the weathered residual pore fissure water occurs in the bedrock full-strong weathering layer, and the bedrock fissure water occurs in the bedrock weathering fissure and structural fissure below the fragmented strong weathering zone. The representative section vault has a pressure head height of 33.19 meters.

2.2 Establishment of seepage model

The issue of groundwater seepage and excess pore water pressure dissipation in porous permeable materials, like soil and rock, is examined using the finite element software SEEP/W. Users can analyze anything from straightforward saturated steady-state problems to intricate saturated-unsaturated time-varying problems thanks to its clear and thorough description.

2.2.1 model parameters

The transient seepage model of the segment structural plane is established using SEEP/W software in accordance with the engineering geological and hydrogeological

Table 1 Model calculation parameters

Material name	Concrete permeability coefficient $K^*(m \cdot d^{-1})$	Volumetric water content w	Residual volume water content w_R	Volume compressibility $m_V(kPa)$	Longitudinal dispersion α_L	Lateral dispersion α_T	Concrete hydraulic conductivity $D\ (m \cdot s^{-1})$
Segment concrete	1.11456×10^{-6}	0.001	0.0001	1.0×10^{-6}	0.04	0.04	4.8×10^{-12}
Rubber	0	2.2	0.001	0.001	0.04	0.04	0
Contact surfaces	0	——	——	——	0.04	0.04	0
Silt	0.0001	0.11333	0.011333	0.001	100	100	1.0
granular strong weathered granite	1	0.090909	0.0090909	0.001	100	100	1.0
Silty clay	0.01	0.083918	0.0083918	0.001	100	100	1.0

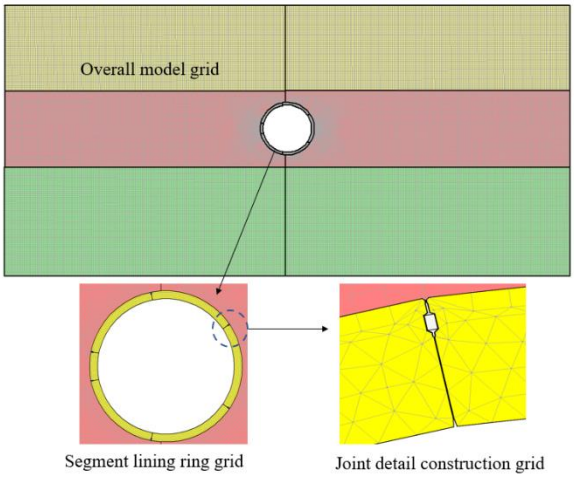

Fig. 4 Computing model grid

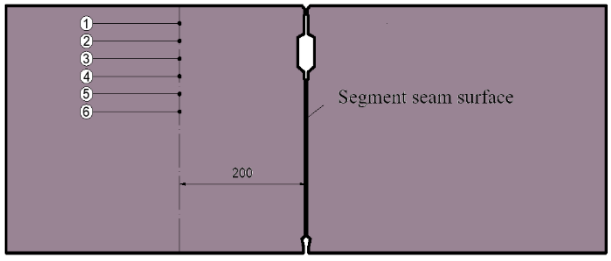

Fig. 5 Segment joint monitoring points schematic diagram (unit: mm)

profiles of representative sections. The convection-dispersion module is then introduced to analyze the coupling between pressure penetration and ion transport. Table 1 displays the model's computation parameters.

2.2.2 Numerical model and computational boundary

The calculation model is shown in Fig. 4. There is no water inflow or outflow on both sides of the tunnel seepage calculation model and the bottom surface of the model, which is defined as the impermeable boundary. The height of the seawater surface from the pressure head of the vault is 33.19 m.

As illustrated in Fig. 5, six monitoring sites that were distant from the segment joints were chosen in order to minimize the effects of bidirectional ion erosion and local seepage field mutation when examining the variation in chloride ion content in segment concrete.

3. Analysis of seepage field change and ion migration law in segment of submarine shield tunnel

Owing to the shield tunnel segment lining structure's transverse and longitudinal staggered segment joints, it is highly likely that during operation, the segment joints will leak water and accelerate the segment joints' corrosion and deterioration due to the aging of the waterproof rubber, construction and assembly errors, and operating dynamic and static loads. Therefore, it is necessary to study the migration and transformation of corrosive ions in the segment of a typical shield tunnel section under general seawater environment (chloride ion content of 0.6%). Assuming that after 30 years of service, leakage occurs at the joints of segment No. 1,2 and 3 (leakage rate of 0.1 $L/(m^2 \cdot d)$).

3.1 Variation law of seepage field

Fig. 6 shows the results of the seepage field distribution inside the segment lining after water leakage occurs at the segment joints at different positions.

The corrosive seawater exhibits the evolution characteristics of continuous seepage from the tunnel's exterior to its interior, as seen in Fig. 6. Local concentration features are present in the seepage field in the joint leakage area, and there is a notable increase in both the depth and range of seepage. Simultaneously, the sequence of erosion depth at the tunnel position is determined to be: vault<haunch< springing. This is because the seawater pressure at the springing is higher than that of the vault and haunch, which gives ion erosion more force. Furthermore, the ion penetration depth away from the joint leakage influence range is found to be uniform, and the leakage gap's penetration depth is not mutated.

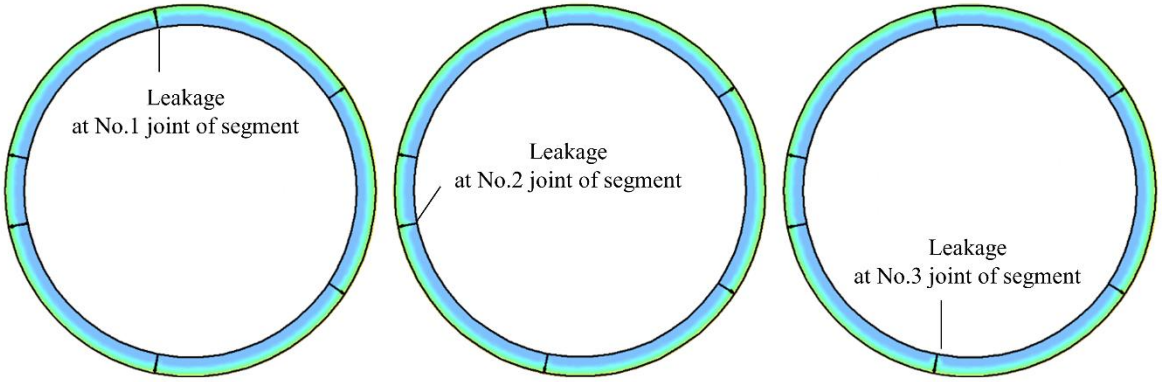

(a) Cloud image of segment seepage field

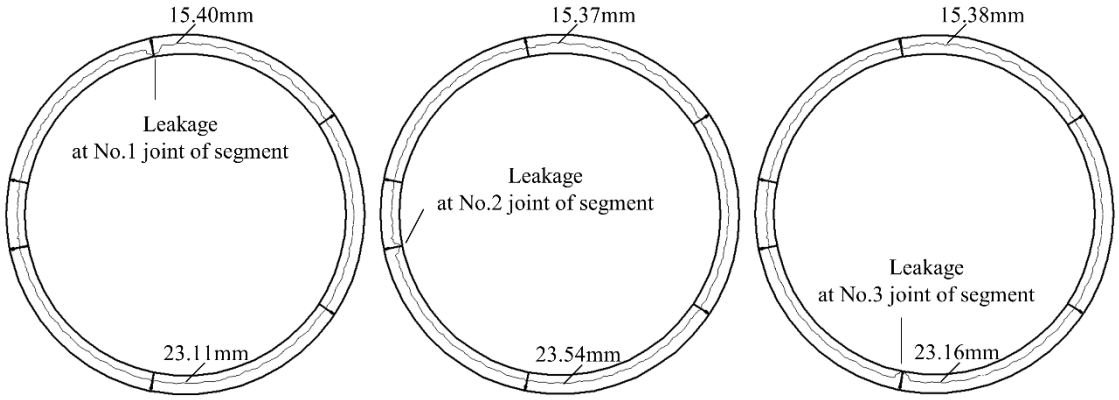

(b) 100a penetration depth indication

Fig. 6 Internal seepage distribution diagram of segment lining under different conditions (100a)

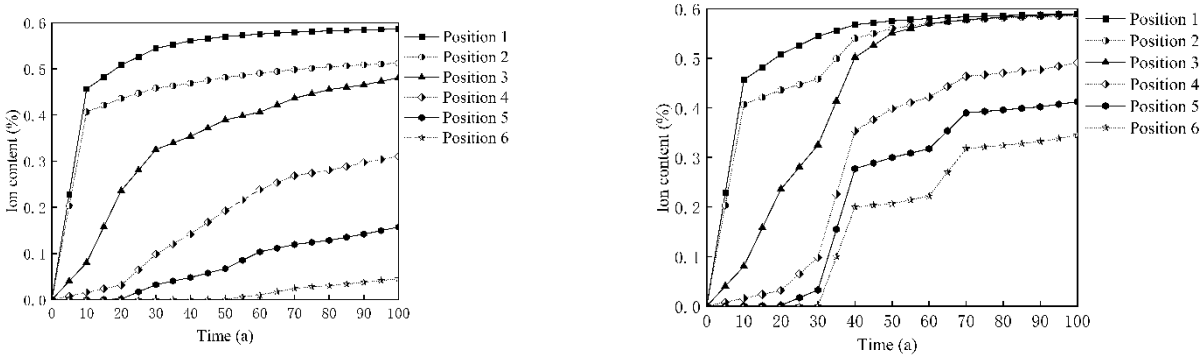

(a) The joint is in good condition without water leakage (b) Leakage at No.1 vault joint

Fig. 7 Vertical distribution curve of ion content at No.1 joint of segment

3.2 Ion content distribution law

Figs. 7-12 illustrate the distribution of ion content in the joint portion and the lining of the Whole ring segment under the conditions of a healthy joint and joint leakage.

Figs. 7-12 shows that the chlorine ion distribution in the joint area is more concentrated when the segment joint leaks. Leakage from the segment joint will exacerbate the joint's erosion range and degree, while the joint without leakage does not increase the joint's chlorine ion distribution range. Comparing the non-leakage state and leakage state of the segment joints, after 30 years of leakage, the chlorine ion content at the segment joints increases suddenly and reaches a higher level earlier than in

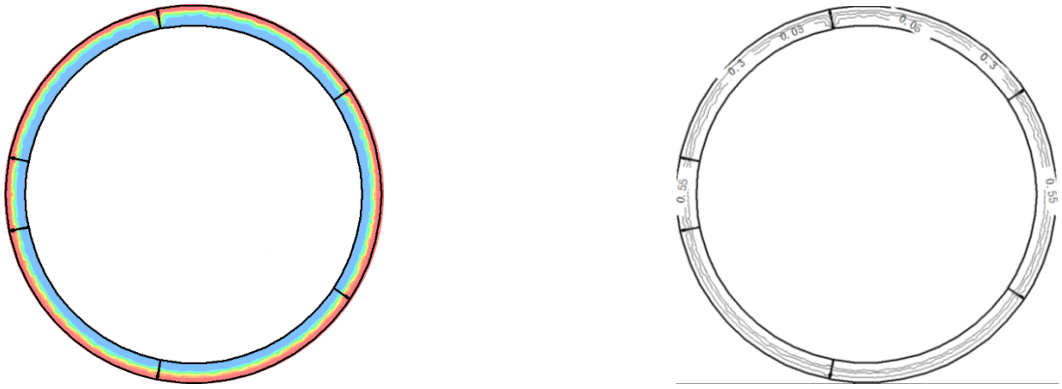

(a) Ion content distribution (b) Ion content equipotential diagram

Fig. 8 Distribution of ion content in segment under leakage condition at No.1 joint of segment (100 years)

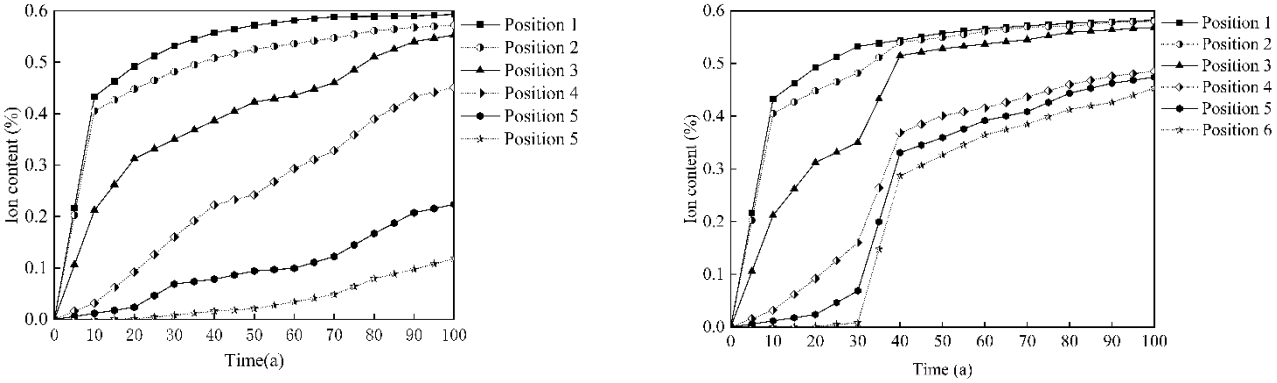

(a) The joint is in good condition without water leakage (b) Leakage at No.2 hance joint

Fig. 9 Vertical distribution curve of ion content at No.2 joint of segment

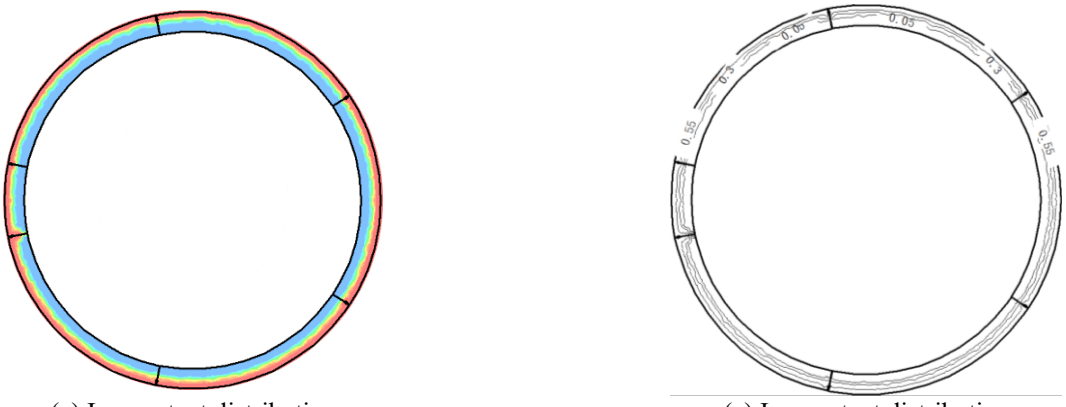

(a) Ion content distribution (a) Ion content distribution

Fig.10 Distribution of ion content in segment under leakage condition at No.2 joint of segment (100 years)

the non-leakage state. While joint leakage has little effect on the position away from the joint, it is evident that it has a significant impact on the chlorine ion erosion in the segment's joint area, which will speed up the segment's and the joint's corrosion deterioration. Concurrently, the rate of chlorine ion content increase tends to be the same at each monitoring point as service time increases.

4. Structural safety analysis considering the effective bearing thickness of submarine shield segment

The spatial state method is used to establish the mathematical model of the mechanical response of the lining, which is based on the theory of curved beam on

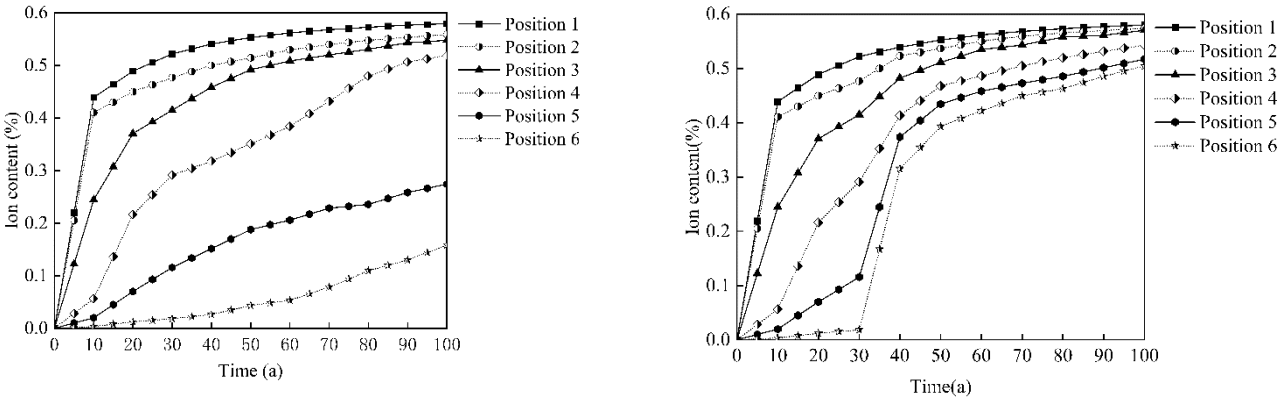

(a) The joint is in good condition without water leakage (b) Leakage at No.3 springing joint

Fig. 11 Vertical distribution curve of ion content at No.3 joint of segment

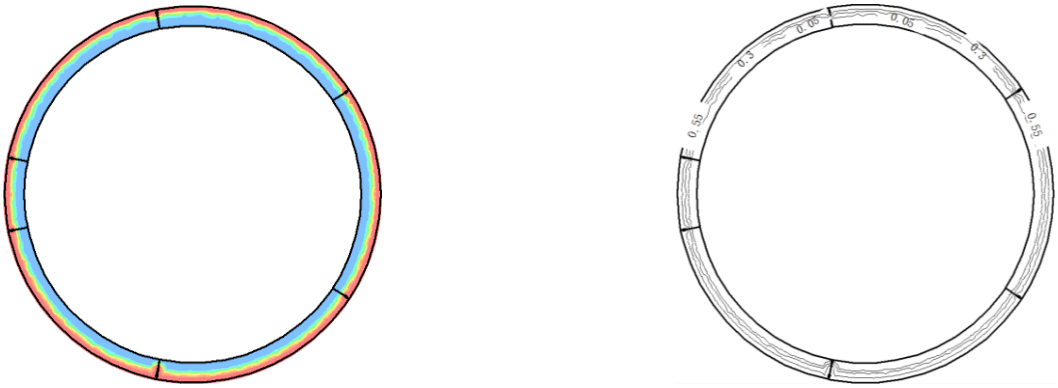

(a) Ion content distribution (b) Ion content distribution

Fig. 12 Distribution of ion content in segment under leakage condition at No.3 joint of segment (100 years)

elastic foundation. The model, which is compared and verified with the numerical model, is analyzed using the Laplace transform. The safety of the lining structure under varying damage location, damage range, and damage degree is investigated by lowering the section height of the curved beam in the local range.

Thus, the chlorine ion content and erosion depth in the segment are obtained, and the thickness of the segment that can withstand the pressure is determined, based on the chlorine ion erosion state during the shield tunnel project's service period in the cross-sea section of the submarine shield tunnel. The structural safety of the ion-eroded shield segment is examined using the analytical solution method, which serves as a foundation for making decisions about the shield tunnel's operational safety.

4.1 Analytical solution of elastic foundation beam model

4.1.1 Model establishment and basic assumptions

Following the submarine shield tunnel's excavation, the surrounding rock frequently experiences significant deformation, allowing the shield tunnel segment and the surrounding rock to fit closely (Liu *et al*. 2020). The shield tunnel segment can analogously be thought of as a curved beam supported on an elastic foundation. Because of the corrosive ions in seawater, the segment's thickness will deteriorate to varying degrees. The tunnel section will gradually transform from a uniform ring of equal thickness to a "toothed" stepped continuous curved beam. As such, its mechanical model can be considered as a stepped curved beam on an elastic foundation (Fig. 13), and the shield tunnel contour's center is used to establish the pole of the polar coordinate system. The location and degree of thickness loss are divided into L_1~L_{2n} segments based on the lining's geometric curvature. Among them, c_i is the loss thickness and h_0 is the design thickness of the lining without deterioration. Any segment of the lining has an effective bearing thickness of h_0-c_i, a radius of R_i, and a thickness loss range of d_i.

Taking into account the previously described circumstances, the following assumptions are formed: 1) the surrounding rock satisfies the Winkler elastic foundation beam model. 2) The shield tunnel segment can be regarded as Euler curved beam, which conforms to the plane section assumption, and the shield tunnel segment material meets the linear elastic requirements. 3) Ignore the error of centroid axis offset caused by cross section mutation.

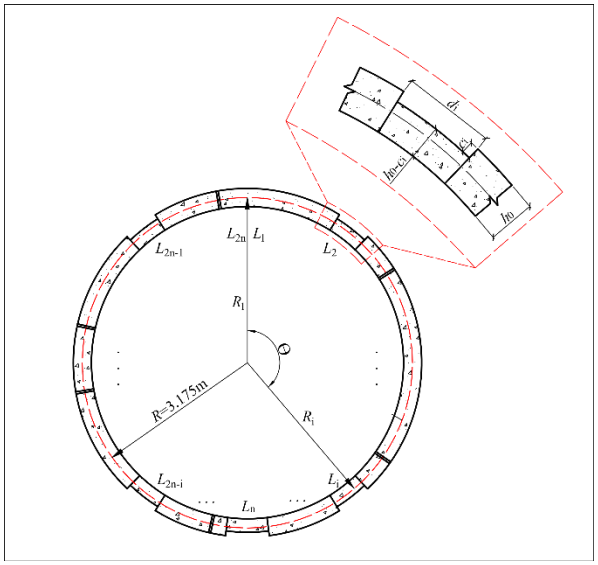

Fig. 13 Segment thickness loss model

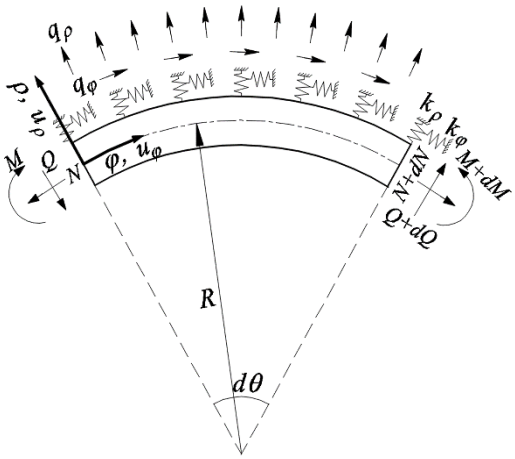

Fig. 14 Microelement force diagram of curved beam on elastic foundation

4.1.2 Analysis of curved beam model on elastic foundation

Fig. 14 displays the force condition after a segment of the segment's micro-element $Rd\theta$ is removed. A local coordinate system is established, where the ρ and φ directions are radial and tangential directions, respectively, and the displacements in the corresponding directions are u_ρ and u_φ. The cross-sectional area of the segment is A, the moment of inertia is I, the radius of the neutral surface is R, the bending moment of the section is M, the shear force is Q, the axial force is N, the radial and tangential spring coefficients are k_ρ and k_φ, respectively. The radial load acting on the micro-element is q_ρ, and the tangential load is q_φ. Fig. 14 displays each vector's positive direction.

The rotation angle and tangential strain of the curved beam can be caused by both tangential displacement and radial displacement, according to the Euler curved beam theory (Wang *et al*. 2020). As a result, the annular strain ε_φ at the middle surface and the rotation angle φ of the curved beam should be as follows

$$\varphi = \frac{1}{R}\frac{du_\rho}{d\theta} - \frac{u_\varphi}{R} \tag{1}$$

$$\varepsilon_\varphi = \frac{1}{R}\frac{du_\varphi}{d\theta} + \frac{u_\rho}{R} \tag{2}$$

Assumption (3) makes clear that the average stress of the section should match the axial stress at the middle surface, and that the axial stress satisfies the linear distribution in the section height. Furthermore, the lining material is linear elasticity, which is consistent with the theoretical field of elastic mechanics (Lv *et al*. 2019), Consequently, the section's axial force is

$$N = E\varepsilon_\varphi A = \frac{EA}{R}\left(\frac{du_\varphi}{d\theta} + u_\rho\right) \tag{3}$$

Both axial force and bending moment will cause the micro-element's rotation angle to change. The axial force reduces the micro-element's rotation angle, whereas the bending moment increases it (the rotation angle is the same as the positive direction of the bending moment). According to the mechanics of materials (Wang and Kang 2022), the change of bending moment and axial force to the rotation angle is 1 and 2 on the right side of Eq. (4) respectively

$$\frac{d\varphi}{d\theta} = \frac{MR}{EI} - \frac{N}{EA} \tag{4}$$

Since h is much smaller than R, $R_1 \approx R$ can be approximately considered. According to the force balance equation of the micro-element in Fig. 14, the following equation can be obtained after omitting the higher-order micro-quantity

$$\frac{dN}{d\theta} = -Q + k_\varphi R u_\varphi - q_\varphi R \tag{5}$$

$$\frac{dQ}{d\theta} = N + k_\rho R u_\rho - q_\rho R \tag{6}$$

$$\frac{dM}{d\theta} = -QR \tag{7}$$

The pressure in the stress analysis of shield tunnel segments is represented by the rectangular coordinate system as horizontal load q_x and vertical load q_y, while q_φ and q_ρ are represented by polar coordinates. As a result, the coordinate transformation formula indicates that there are

$$q_\rho = -q_y \cos^2\theta - q_x \sin^2\theta \tag{8}$$

$$q_\varphi = (q_y - q_x)\cos\theta\sin\theta \tag{9}$$

The absolute values of the horizontal and vertical pressures on shield tunnel segments are denoted by the formulas q_x and q_y, respectively.

The shield tunnel's contour is circular, and water pressure is applied to the subsea tunnel's exterior side with the direction of the pressure directed toward the circle's center. The water pressure calculation formula is derived to make the process of calculating the water pressure outside the shield tunnel easier. The distance between the tunnel vault and the sea level is the height of water head h, and the calculation radius of shield lining is R. When the position angle of the calculated water pressure is θ, the water pressure on the segment is

$$q_w = r_w\left[h + R(1-\cos\theta)\right] \tag{10}$$

The tunnel is on the seabed. Considering the effect of water pressure, the calculation formulas of q_φ and q_ρ are as follows

$$q_\rho = -q_y \cos^2\theta - q_x \sin^2\theta - r_w\left[h + R(1-\cos\theta)\right] \tag{11}$$

$$q_\varphi = (q_y - q_x)\cos\theta\sin\theta \tag{12}$$

The internal force and displacement are dual when the space state approach is applied (Huang *et al.* 2020), and the first-order equations' matrix form is obtained

$$\frac{dS}{d\theta} = DS + f \tag{13}$$

S is the mechanical response matrix:

$$S = \begin{bmatrix} u_\rho & u_\varphi & \varphi & M & Q & N \end{bmatrix}^T$$

In the formula, u_ρ and u_φ are radial and tangential displacements, respectively. φ is the rotation angle of lining section; M is the section bending moment; Q is the section shear force; N is the cross-section axial force.

D is the coefficient matrix:

$$D = \begin{bmatrix} 0 & 1 & R & 0 & 0 & 0 \\ -1 & 0 & 0 & 0 & 0 & R/EA \\ 0 & 0 & 0 & R/EI & 0 & -1/EA \\ 0 & 0 & 0 & 0 & -R & 0 \\ k_\rho R & 0 & 0 & 0 & 0 & 1 \\ 0 & k_\varphi R & 0 & 0 & -1 & 0 \end{bmatrix}$$

In the formula, E is the elastic modulus of segment concrete; A is the cross-sectional area of lining; I is the moment of inertia of the cross section; k_ρ and k_φ are radial and tangential spring coefficients, respectively.

$\boldsymbol{f}$ is the external load matrix of lining:

$$f = \begin{bmatrix} 0 & 0 & 0 & 0 & -q_\rho R & -q_\varphi R \end{bmatrix}^T$$

The Laplace transform and inverse transform of Formula (13) are obtained

$$S(\theta) = L^{-1}[(Is - D)^{-1}]S(0) + L^{-1}[(Is - D)^{-1}T(\theta)] \tag{14}$$

$S(0)$ is the initial state physical quantity of the mechanical response matrix; I is a sixth-order unit matrix; s is the mapping variable of θ; $T(\theta)$ is the image function of f; L^{-1} is the sign of Laplace inverse change.

Simplify the expression and get the formula (17)

$$\overline{D} = L^{-1}[(Is - D)^{-1}] \tag{15}$$

$$\overline{f}(\theta) = L^{-1}[(Is - D)^{-1}T(\theta)] \tag{16}$$

$$S(\theta) = \overline{D}S(0) + \overline{f}(\theta) \tag{17}$$

4.1.2 Analysis of effective bearing thickness loss of segment on elastic foundation

The calculation method of shield tunnel structure adopts the homogeneous ring method. This method assumes that the bending stiffness of the whole segment of the shield is uniform, regardless of the flexible characteristics of the segment joint position and the decrease of bending stiffness. Consequently, because of variations in load forms, material deterioration, and curvature changes, the whole ring segment is split into n segments. Through the rigid connection, the internal force and displacement of the section change continuously. $L_{i,0}$ represents the beam L_i's initial end, and $L_{i,1}$ represents its end. The transfer equation of the deformation and internal force of the segment between the curved beams is

$$S_{i,0} = S_{i-1,1} \tag{18}$$

$S_{i,0}$ is the mechanical response matrix at the beginning of the i curved beam; $S_{i\text{-}1,1}$ is the mechanical response matrix at the end of the i-1 curved beam.

It can be seen from Formula (17) that the transfer equation of deformation and internal force in curved beam L_i is

$$S_i(\theta) = \overline{D}S_{i,0} + \overline{f}(\theta) \tag{19}$$

The deformation and internal force of any section of the whole ring segment containing the initial mechanical response matrix $S_{1,0}$ of the first curved beam can be calculated by combining Formulas (18) and (19)

$$\begin{aligned} S_i(\theta) &= \overline{D}_i S_{i-1,1} + \overline{f}_i(\theta) = \overline{D}_i[\overline{D}_{i-1}S_{i-1,0} + \overline{f}_{i-1}(\theta)] + \overline{f}_i(\theta) \\ &= \cdots = \left(\prod_{j=1}^{i}\overline{D}_j\right)S_{1,0} + \sum_{j=1}^{i}\left(\prod_{k=1}^{j}\overline{D}_k\right)\overline{f}_{k-1}(\theta) + \overline{f}_i(\theta) \end{aligned} \tag{20}$$

As a closed structure, although the whole ring segment is divided into 2n curved beams, the end of the section is connected and the deformation is coordinated. Therefore, the internal force and deformation of the end of the 2n curved beam and the beginning of the first curved beam are equal.

Table 2 Physical and mechanical parameters of strata

Strata name	natural density ρ (g/cm^3)	specific gravity d_s	void ratio e	Cohesion c/ kPa	internal friction angle φ/°
Silt	1.59	2.76	1.890	10	3
granular strong weathered granite	2.00	2.71	0.582	30	25
Silty clay	1.96	2.72	0.707	30	14

$$S_{2n,1} = S_{1,0} \tag{21}$$

Formula (21) Substituted into formula (20), the matrix $S_{1,0}$ can be solved

$$S_{1,0} = \frac{\sum_{j=1}^{2n}\left(\prod_{k=1}^{j}\overline{D}_k\right)\overline{f}_{k-1}(\theta)+\overline{f}_{2n}(\theta)}{I-\prod_{j=1}^{i}\overline{D}_j} \tag{22}$$

Substituting Formula (22) into Formula (20), the displacement and deformation of any section of the segment can be obtained.

4.2 Structural calculation load

The weight of the segment and the horizontal resistance of the stratum are taken into consideration in the design of the shield segment, while the top and bottom of the tunnel are regarded as uniform loads and the side of the tunnel as linear loads (Feng *et al*. 2018, Gong and Ding 2018). The underwater granular strong weathered granite stratum, which is covered in mucky soil, is where the shield tunnel is situated. Elastic resistance can be disregarded when calculating the force of the shield tunnel whole ring segment using the free deformation elastic homogeneous ring method.

The safety verification of the segment structure needs to consider the load comprehensively. According to the survey data of the stratum, the physical and mechanical parameters of the stratum are shown in Table 2.

$$S_{1,0} = \frac{\sum_{j=1}^{2n}\left(\prod_{k=1}^{j}\overline{D}_k\right)\overline{f}_{k-1}(\theta)+\overline{f}_{2n}(\theta)}{I-\prod_{j=1}^{i}\overline{D}_j} \tag{23}$$

Substituting Formula (22) into Formula (20), the displacement and deformation of any section of the segment can be obtained.

4.2 Structural calculation load

The weight of the segment and the horizontal resistance of the stratum are taken into consideration in the design of the shield segment, while the top and bottom of the tunnel are regarded as uniform loads and the side of the tunnel as linear loads (Feng *et al*. 2018, Gong and Ding 2018). The underwater granular strong weathered granite stratum, which is covered in mucky soil, is where the shield tunnel is situated. Elastic resistance can be disregarded when calculating the force of the shield tunnel whole ring segment using the free deformation elastic homogeneous ring method.

The safety verification of the segment structure needs to consider the load comprehensively. According to the survey data of the stratum, the physical and mechanical parameters of the stratum are shown in Table 2.

$$S_{2n,1} = S_{1,0} \tag{24}$$

R is the tunnel radius; c is soil cohesion; φ is internal friction angle of stratum; H is the distance from the tunnel vault to the earth's surface; γ is the weight by volume of the dominant stratum, and the stratum is assumed to be a single stratum for calculation; λ is the lateral pressure coefficient, take λ=1; e is a constant, take 2.71828183.

It is calculated that h_0=-1.9753 m, which is less than twice the hole diameter, so the final vertical load calculation height h0 = 4.086 m. The weight by volume of the dominant stratum γ=6.7739 KN/m^3, vertically uniform loose earth pressure of surrounding rock q=γh_0=27.678KN/m^2, the horizontal uniform loosening pressure e of surrounding rock can be calculated according to Rankine formula, e=25.303 KN/m^2.

The vertical subgrade reaction is computed by keeping the segment force balance intact and figuring out the reaction force associated with other loads. Assuming that it is evenly distributed, the vertical subgrade reaction F_R is calculated, F_R=23.8KN/m^2. The load calculation diagram of the structure is shown in Fig. 15.

4.3 Analytical solution verification and analysis

The internal force and displacement of the shield tunnel section are calculated using the homogeneous ring method in conjunction with the shield tunnel load using a self-designed Matlab code. With reference to the foundation spring resistance coefficient value found in the 'Guidelines for Design of Highway Tunnel' the radial spring resistance coefficient is k_ρ=200 MPa/m, while the tangential spring resistance coefficients are k_φ=0 and k_φ= k_ρ/3 respectively. After applying the above parameters to solve, the top spring tension zone is found through one to two trial calculations, and the tension zone's spring stiffness is zero. Simultaneously, as illustrated in Figure 16, the mechanical calculation results of the numerical analysis software (ANSYS) under the same working conditions are compared to confirm the validity of the analytical solution.

Fig. 16 compares the axial force and bending moment of segment under the two working conditions of k_φ=0 and k_φ= k_ρ/3 between the analytical solution and the ANSYS numerical solution in the range of [0 °, 180°]. As can be seen, there is a good degree of agreement between the two

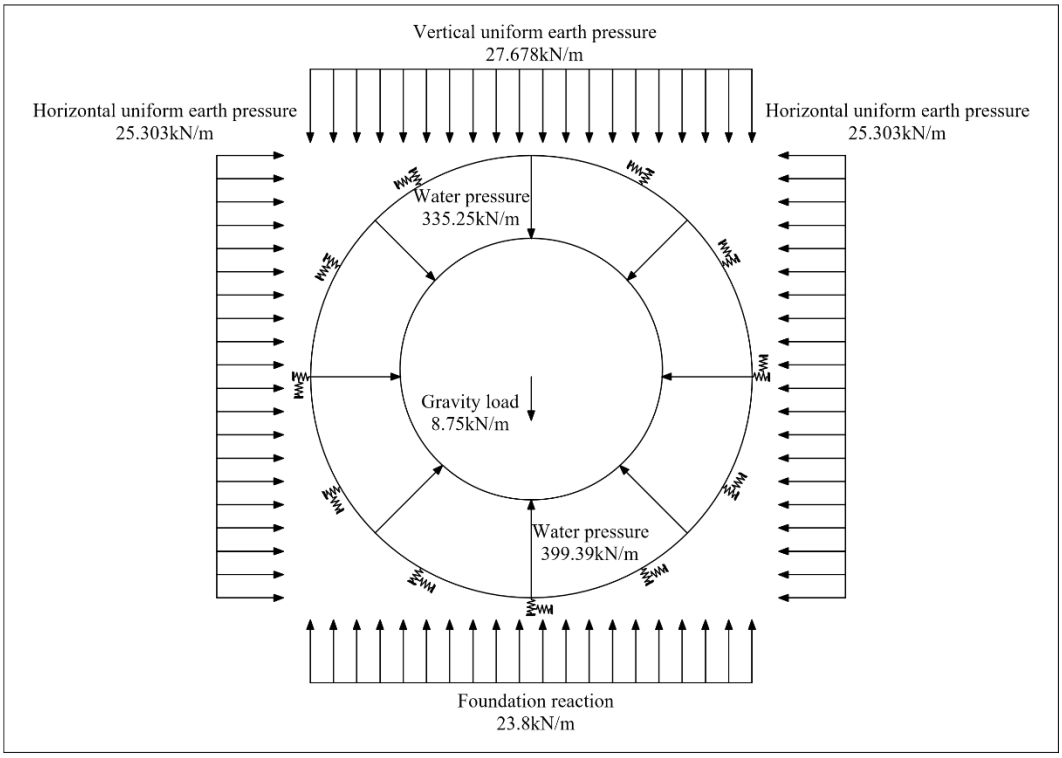

Fig. 15 Structural force diagram of submarine shield tunnel

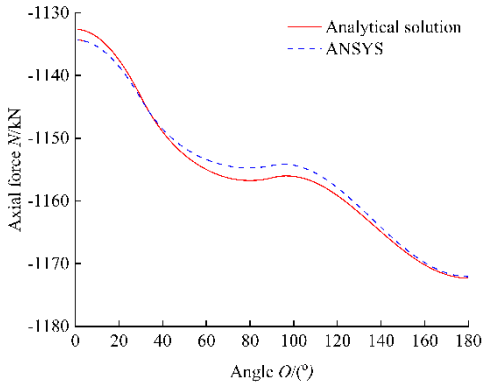

(a) Axial force of segment with k_φ=0

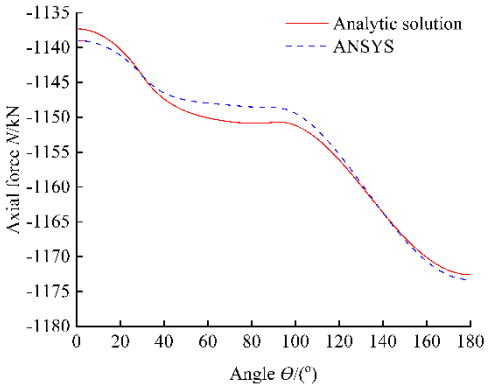

(b) Axial force of segment with $k_\varphi = k_\rho/3$

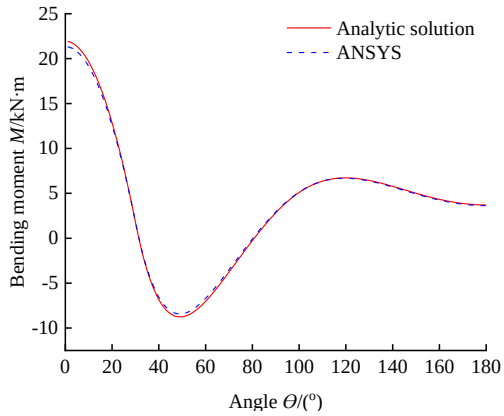

(c) The bending moment of segment with k_φ=0

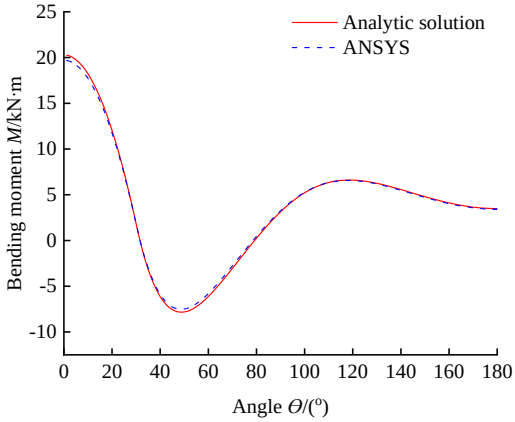

(d) The bending moment of segment with $k_\varphi = k_\rho/3$

Fig. 16 Comparison of analytical solution and ANSYS numerical solution

methods' results. When k_φ=0 and k_φ= k_ρ/3, with the increase of the value of θ, the axial force generally shows an increasing trend, while the bending moment shows a wavy change. At the same time, the axial force corresponding to different tangential spring coefficients is basically the same as the value of θ increases, and the change trend of the corresponding bending moment is basically the same. The global maximum value of positive bending moment appears at the vault. The value of the bending moment is 21.92 kN·m when k_φ=0, and the value of the bending moment is 20.23 kN·m when k_φ= k_ρ/3. At the haunch (θ=49), the global maximum value of negative bending moment is observed. The value of the bending moment is -8.76 kN·m when k_φ=0, and the bending moment is -7.84 kN·m when k_φ=k_ρ/3. The local maximum value of positive bending moment appears at the springing (θ=120°). When k_φ=0, the bending moment is 6.72 kN·m, and when k_φ= k_ρ/3, the bending moment is 6.6 kN·m.

The maximum axial force is 1172 kN and the minimum is 1132 kN calculated by the analytical solution. As a typical eccentric compression member, the coupling of axial force and bending moment affects the segment's bearing capacity. Consequently, the most hazardous parts of the shield tunnel are the vault, haunch and springing (Wei 2021). As seen in Fig. 2, the shield tunnel simultaneously possesses the properties of several joints. Joint leakage can easily result in the loss of effective bearing thickness, which can lead to the failure of structural bearing capacity. Therefore, the range and degree of thickness loss are calculated and analyzed for the above three positions of vault, haunch and springing (the haunch and springing are taken from the left position of the shield tunnel).

4.4 Safety analysis of effective bearing thickness loss of shield tunnel

4.4.1 Calculated work condition

The segment concrete's 0.3% corrosion threshold is used. The segment corrodes and starts to lose its effective bearing thickness when the Cl-ion content in the shield segment reaches 0.3%. In accordance with the research content of Chapter 2, the Cl^-ion content in the segment of the specific year can be obtained to determine whether the segment is corroded, and the most unfavorable situation can be considered to determine the effective bearing thickness loss.

The calculation uses the model shown in Fig. 15. The research mainly discusses the change law of safety factor under the condition of effective bearing thickness loss of lining. Therefore, part of the load shared by the grouting layer behind the wall is ignored, and the tangential spring stiffness k_φ is taken as k_ρ/3 (He *et al*. 2021). According to the 'Code for Design of Road Tunnel'，the safety factor calculation formula is as follows when the compressive strength of the concrete lining controls the safety factor

$$KN \le \varphi \alpha R_a bh \tag{25}$$

$$\alpha = 1 + 0.648\frac{e}{h} - 12.569(\frac{e}{h})^2 + 15.444(\frac{e}{h})^3 \tag{26}$$

When controlled by tensile strength, the calculation formula of safety factor is

$$\mathrm{KN} \le 1.75\mathrm{R_l bh} / (\frac{6\mathrm{e}}{\mathrm{h}} - 1) \tag{27}$$

K is the safety factor; N is the axial force; M is bending moment; φ is the longitudinal bending coefficient of the component, and the shield tunnel can be taken as 1; α is the eccentric influence coefficient of the axial force, which can be determined according to the empirical formula (26). e is the eccentricity; R_a is the ultimate compressive strength of concrete or masonry; b is the width of the cross section; h is the thickness of the cross section; R_l is the ultimate tensile strength of concrete or masonry.

4.4.2 The impact of the shield segment's effective bearing thickness loss on the safety factor

The yield of the section in a concrete structure is typically identified by the shape of a plastic hinge. Given that concrete is typically brittle, once it yields, it will be quickly destroyed. As a result, the yield state can also be approximately replaced by the section's ultimate bearing state. The formula for calculating the tunnel lining's safety factor is provided by the 'Code for Design of Road Tunnel'. When the safety factor K=1, it is the ultimate bearing state of the segment section, so it can be judged whether the section is yielding by calculating the safety factor of the segment.

The shield tunnel is an arch structure with multiple statically indeterminate due to the surrounding rock's constraints. The shield tunnel will become an unstable system once the number of yield sections exceeds the structural limitations. The critical state is the ultimate bearing state of the shield tunnel. There is no definite value of the yield section of the segment when it enters the limit state. It is considered that the shield tunnel has reached the limit bearing state when there are three yield sections in the structure.

Seawater corrosion causes the segment's effective bearing thickness to decrease as service time increases. Fig. 17 illustrates the variation of the joint position's safety factor.

Fig. 17 shows that as the year increases, the safety factor of the shield segment's three joint positions decreases. Using the example of Fig. 17(a), the safety factor drops from 16.44 to 12.02 when the joint is intact and from 16.44 to 5.04 when the joint leaks. We can conclude that the segment's safety factor drops more when the joint leaks than when it is intact. The corrosive ions can come into contact with the inside of the segment through the joint when it leaks. As a result, the segment's effective bearing thickness is lost more and the safety factor decreases when the joint leaks. Under the two conditions of intact joint and joint leakage, the safety factor of shield tunnel has the same change rule within 30 years after the shield tunnel began to serve, but the corrosive ions continue to erode the joint before the leakage of the segment joint, resulting in the safety factor is slightly smaller than the safety factor when the segment joint is intact at the same time. After 30 years of service in the tunnel, the safety factor of the segment

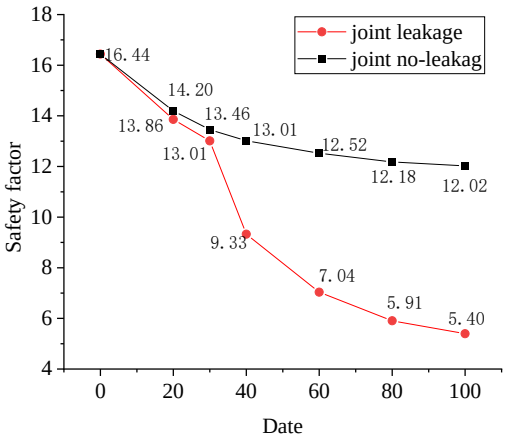

(a) Change of safety factor at No.1 joint

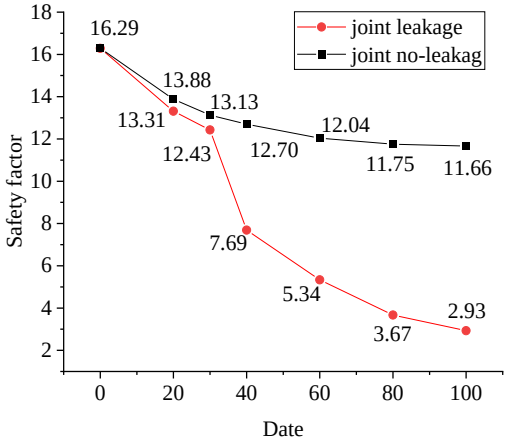

(b) Change of safety factor at No.2 joint

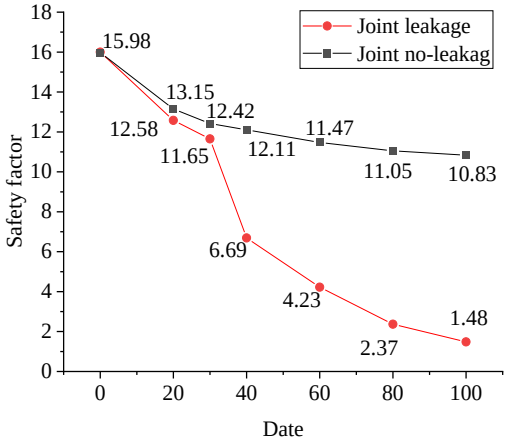

(c) Change of safety factor at No.3 joint

Fig. 17 The influence of effective bearing thickness loss on the safety factor of segment

plummeted due to the leakage of the joints. Simultaneously, the rate of increase of ion content is trending downward. This is because the concentration gradient and pressure gradient have an impact on the erosion ion migration in the segment. The segment's rate of corrosion thickness increase is reducing due to a decrease in the transmission rate of erosion ions to the inner side of the segment. The safety factor's change rate falls, based on the safety factor calculation algorithm. It is possible to say that the shield tunnel reaches its ultimate bearing state when there are three yield sections present. The safety factor at the leakage of the No. 3 joint is the global minimum when compared to other positions in the segment. Fig. 17(c) shows that the calculated shield tunnel section has a sufficient safety guarantee because, in 100 years, the minimum safety factor at the segment's No. 3 joint is 1.48 and the safety factor is greater than 1.

The research results are only the cross section corresponding to the highest point at the top of the shield tunnel 33.19 m from the sea level. However, the longitudinal section of the shield tunnel of the cross-sea section of Xiamen Rail Transit Line 2 is V-shaped slope, and the distance from the highest point at the top of the tunnel to the highest water level of the sea surface is about 48.3 m, the above research results are not sufficient for the safety of the tunnel. Therefore, the variation law of safety of No. 3 joint leakage of shield segment is discussed based on the research mentioned above, assuming different water depths. The water depths are assumed to be 40m, 60m, 80m and 90m respectively. The shield tunnel is determined to be a deep buried tunnel by Section 3.2 'structural calculation load'. The calculation method is commonly used in the Terzaghi formula. The vertical load calculation is determined by the average height of the surrounding rock collapse. According to the engineering conditions, the calculated average height of the collapse is very small. At the same time, the calculated seawater pressure is about 17 times the loose earth pressure of the surrounding rock. Therefore, the change of the loose earth pressure can be ignored. The loose earth pressure calculated by the cross section of the tunnel used in the above study is calculated as the assumed working condition. The load calculation is calculated by matlab self-compiled code, and the safety factor change near the No.3 joint (197°) is shown in Fig. 18.

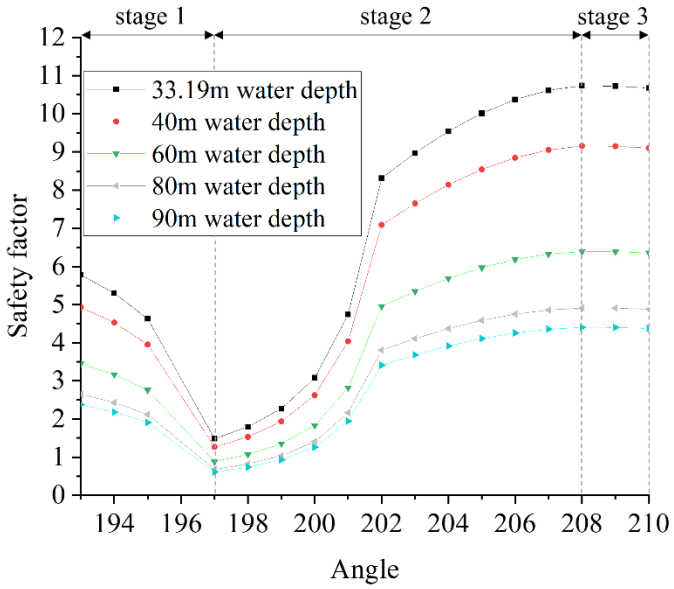

Fig. 18 The change of safety factor near the joint during the leakage of No.3 joint under different water depths

Fig. 18 illustrates how the safety factor continuously decreases at the same segment position as the water depth increases and how it exhibits a similar change rule at varying water depths. The change curve of the safety factor is similar to the three-stage distribution curve of the 'spoon-shaped'. This phenomenon is caused by the fact that the bending moment exhibits the law of convex quadratic parabola reduction, but the axial force essentially stays constant as the angle increases. At this point, the eccentricity and the bending moment decrease synchronously. The ultimate bearing capacity is enhanced and the impact of eccentricity is lessened when the cross-section size remains constant. As a result, the second stage's safety factor is raised. During the first stage, there is a notable decrease in the safety factor due to the segment's relatively large cross-sectional area and reduced eccentricity. The third stage is characterized by little changes in the bending moment and a generally stable safety factor.

Following computation, the safety factors are less than one at 197°,198° and 199°(Location near No.3 joint) when the water depth reaches 90 m and the safety factors of shield segment is 0.60825,0.73618 and 0.93072 at those positions. The tunnel section reaches the ultimate bearing state when the segment structure has three yield sections. As a result, it is evident that the cross-sea portion of the Xiamen Rail Transit Line 2 shield tunnel has enough safety to ensure both the people's safety and the safe operation of the tunnel

5. Conclusions

SEEP/W software is used to establish the segment structural plane's transient seepage model. The erosion deterioration mechanism of the whole ring segment of the shield segment in the subsea tunnel under unsaturated state is studied, and the loss degree of the effective bearing thickness of the segment is judged, based on the convection-diffusion coupling theory. The mathematical calculation model of the lining mechanical response is built using the spatial state method, and the analytical solution of the lining mechanical response is derived, all based on the curved beam theory of elastic foundation. The equation's validity is confirmed by the fact that the computation results are essentially consistent with the ANSYS software's simulation results. Then it is applied to the tunnel safety state evaluation under the condition of effective bearing thickness loss of segment. The main conclusions are as follows:

- Seawater continuously percolates from the segment's exterior into its interior, getting deeper and deeper. The segment's ion content rises in tandem with the tunnel's extended service time. Corrosive seawater presents the evolution characteristics of continuous seepage from the outside to the inside of the tunnel. There is a discernible increase in seepage depth and range in the vicinity of the joint leakage, and the seepage field exhibits the features of local concentration. The further one is from the outer surface of the tunnel, the lower the ion content becomes.
- In comparison to the tunnel vault, the tunnel arch foot structure bears more seawater pressure and the ion erosion is more serious. The whole ring segment presents the characteristics of uneven corrosion. Corrosion monitoring equipment can be installed in the vulnerable parts such as tunnel arch foot to monitor the change of ion content in real time. According to the monitoring data, the waterproof and anti-corrosion measures can be adjusted in time. At the same time, the lining structure is made of materials with better corrosion resistance to improve its resistance to ion erosion.
- Corrosive ions in segment concrete may penetrate more readily when water pressure is present. The tunnel's external

water pressure will increase the erosion ions' penetration depth and speed on the segment. The depth of seawater penetration increases with increasing external water pressure. But as service time increases, the gap between the ion content growth rates at each monitoring location is closing. To lessen the rate at which corrosive ions invade the segment, it is therefore recommended that, when creating segments, materials that are resistant to aging and corrosion be used to reinforce the waterproof layer on the outer surface of the tunnel.

- In the later stage of shield segment service, each monitoring point's ion content growth rate is extremely close when segment joint leakage is present. The growth rate of ion content at the monitoring points in the later stage of shield service is significantly different when the segment joints are intact. The joints between the segments should be sealed to increase the tunnel's service life and guarantee safety by lowering the likelihood of seawater seeping through the joints.
- The safety factor of the segment when the joint leaks is less than that when the joint is intact, according to calculations made using the analytical solution. Simultaneously, the segment safety factor will plummet due to joint leakage as compared to the segment joint in its intact state. Simultaneously, both states' rates of change exhibit an overall declining trend. The safety factor at the leakage of the No. 3 joint is the global minimum when compared to other locations in the segment. At the No. 3 joint of the segment, the minimum safety factor is 1.48 when 100 years is taken into account, and the safety factor is greater than 1. Therefore，the computed cross section of the typical shield tunnel has a sufficient safety guarantee.
- The safety factor shows a similar change rule at different water depths and continuously decreases at the same segment position as the water depth increases. The three phases of "sudden drop-rise-stability" are represented by a "spoon-shaped" change rule on the safety factor's change curve. This phenomenon is due to the increase of the angle, the axial force is almost unchanged, but the bending moment is reduced by the convex quadratic parabola, and the ultimate bearing capacity is improved, so the safety factor of the second stage is improved. During the initial phase, there is a notable decrease in the safety factor due to the lining's relatively large cross-sectional area and reduced eccentricity. The third stage is characterized by minimal changes in the bending moment and a generally stable safety factor.
- This paper's analytical solution resolves the issue of the inadequate applicability of indexes in earlier research by allowing the safety factor of any shield tunnel segment to be determined solely by calculating the segment's effective bearing thickness loss degree. The analytical solution calculation results are more conservative because it is assumed that segment concrete cannot be stressed when its corrosive ion content is less than 0.3%. The process of developing the evaluation model indicates that the secondary lining made of molded concrete can also have its safety status assessed using the equation. It is very important for the safe operation of the tunnel and the safety of people's property and has a wide range of applications.

Acknowledgments

This study is supported by the National Natural Science Foundations of China (52374079). The authors gratefully acknowledge these supports.

References

Batany, S., Peyneau, P.E., Lassabatere, L., Bechet, B., Faure, P. and Dangla, P. (2019), "Interplay between molecular diffusion and advection during solute transport in macroporous media", *Vadose Zone J.*, **18**(1), 1-15 https://doi.org/10.2136/vzj2018.07.0140.

Chen, G.H., Zou, J.F. and Qian, Z.H. (2019), "An improved collapse analysis mechanism for the face stability of shield tunnel in layered soils", *Geomech. Eng.*, **17**(1), 97-107. https://doi.org/10.12989/gae.2019.17.1.097.

Dong, B.X., Chieh, C.W., Ong, D.E.L. and Ge, L. (2021), "Evaluation of geological conditions and clogging of tunneling using machine learning", *Geomech. Eng.*, **25**(1), 59-73. https://doi.org/10.12989/gae.2021.25.1.059.

Dong, L., Yang, Y.K., Liu, Z.X., Yang, T., Xue, C.H., Shao, R.Z. and Wu, C.Q. (2024), "Effect of chloride ion migration behaviour on the microstructure and mechanical properties of ultra-high performance concrete: A review", *J. Build. Eng.*, **82**, https://doi.org/10.1016/j.jobe.2023.108233.

Feng, C.Q., Si, X.H., Li, B.T., Cao, L.M. and Zhu, J. (2021), "An inverse problem to simulate the transport of chloride in concrete by time-space fractional diffusion model", *Inverse Probl. Sci. Eng.*, **29**(12), 2429-2445. https://doi.org/10.1080/17415977.2021.1914606.

Feng, K., He, C., Qiu, Y., Zhang, L., Wang, W., Xie, H.M., Zhang, Y.Y. and Cao, S.Y. (2018), "Full-scale tests on bending behavior of segmental joints for large underwater shield tunnels", *Tunn. Undergr. Sp. Tech.*, **75**, 100-116. https://doi.org/10.1016/j.tust.2018.02.008.

Fu, H., Di, W., Nan, X. and Chen, O.R. (2021), "Upper bound limit analysis of blow-out failure mode of excavation face of shield tunnel considering groundwater seepage", *Geomech. Eng.*, **26**(3), 227-234. https://doi.org/10.12989/gae.2021.26.3.227.

Ghasemi, S.H. and Nowak, A.S. (2018), "Reliability analysis of circular tunnel with consideration of the strength limit state", *Geomech. Eng.*, **15**(3), 879-888. https://doi.org/10.12989/gae.2018.15.3.879.

Gong, C.J. and Ding, W.Q. (2018), "A computational framework to predict the water-leakage pressure of segmental joints in underwater shield tunnels using an advanced finite element method", *Int. J. Number. Anal. Mech. Geomech.*, **42**(16), 1957-1975. https://doi.org/10.1002/nag.2839.

Guo, X.F., Li, C. and Huo, T.H. (2021), "A quantitative evaluation method on the stability of roadway surrounding rock in partial confining stress based on plastic zone shapes", *Geomech. Eng.*, **25**(5), 405-415. https://doi.org/10.12989/gae.2021.25.5.405.

He, C. and Feng, K. (2021), "Integral analysis method of large-section shield tunnel structure", Tunnel construction (in English and Chinese), **41**(11), 1827-1848, I0021-I0042. https://doi.org/10.3973/j.issn.2096-4498.2021.11.002.

He, Z.S., He, C., Kang, X.Y., Huang, X. and Wang, S.M. (2023), "Assessment of structural performance of super large cross-section subsea RC shield tunnels: Emphasis on the combined effects of highly hydrostatic pressure and corrosion-induced deterioration", *Ocean Eng.*, **288**. https://doi.org/10.1016/j.oceaneng.2023.116134.

Hodhod, O.A. and Ahmed, H.I. (2014), "Modeling the service life

of slag concrete exposed to chlorides", *Ain Shams Eng. J.*, **5**(1),49-54. https://doi.org/10.1016/j.asej.2013.08.001.

Huang, W.M., Wang, J.C., Xu, R.Q., Yang, Z.X. and Xu, R.Q. (2020), "Structural analysis of shield tunnel lining using theory of curved beam resting on elastic foundation", *J. Zhejiang Univ.*, https://doi.org/10.3785/j.issn.1008-973X.2020.04.018.

JTG D70-2004 (2004), Code for Design of Road Tunnel, China communications press, Beijing, China.

JTG/T D70-2010 (2010), Guidelines for Design of Highway Tunnel, China communications press, Beijing, China.

Kim, N.Y., Park, D.H., Jung, H.S. and Kim, M.I. (2020), "Deformation characteristics of tunnel bottom after construction under geological conditions of long-term deformation", *Geomech. Eng.*, **21**(2), 171-178. https://doi.org/10.12989/gae.2020.21.2.171.

Lei, M.F., Peng, L.M. and Shi, C.H. (2015), "Durability evaluation and life prediction of shield segment under coupling effect of chloride salt environment and load", *J. Central South Univ.*, **46**, 3092-3099. https://doi.org/10.11817/j.issn.1672-7207.2015.08.044.

Liang, X., Qi, T.Y., Jin, Z.Y., Qin, S.J., Chen, P.T. and Liu, Y. (2020), "Risk assessment system based on fuzzy composite evaluation and a backpropagation neural network for a shield tunnel crossing under a river", *Adv. Civil Eng.*, 1-14. https://doi.org/10.1155/2020/8840200.

Liu, B., Yu, Z.W., Hang, Y.H., Wang, Z.L., Yang, S. and Liu, H. (2020), "A simplified combined analytical method for evaluating the effect of deep surface excavations on the shield metro tunnels", *Geomech. Eng.*, **23**(5), 405-418. https://doi.org/10.12989/gae.2020.23.5.405.

Liu, J.K., Jiang, Y.J., Zhang, Y.C. and Sakaguchi, O. (2021), "Influence of different combinations of measurement while drilling parameters by artificial neural network on estimation of tunnel support patterns", *Geomech. Eng.*, **25**(6), 439-454. https://doi.org/10.12989/gae.2021.25.6.439.

Liu, J.K., Luan, H.G., Zhang, Y.C., Osamu, S. and Jiang, Y.J. (2020), "Prediction of unconfined compressive strength ahead of tunnel face using measurement-while-drilling data based on hybrid genetic algorithm", *Geomech. Eng.*, **22**(1), 81-95. https://doi.org/10.12989/gae.2020.22.1.081.

Liu, X.R., Xiong, F., Zhou, X.H., Liu, D.S., Chen, Q., Zhang, J.L., Han, Y.F., Xu, B., Deng, Z.Y. and He, C.M. (2022), "Physical model test on the influence of the cutter head opening ratio on slurry shield tunnelling in a cobble layer", *Tunn. Undergr. Sp. Tech.*, **120**, 104264. https://doi.org/ 10.1016/j.tust.2021.104264.

Liu, Y.K., Wu, Y., Li, W.H., Zhang, Q.S., Tai Liu, R., Bai, J.W. and Li, W. (2024), "Development of a water leakage model test system and investigation of the water leakage behavior in subsea shield tunnels during operation", *Measurement*, 233. https://doi.org/10.1016/j.measurement.2024.114691.

Lv, J.B., Li, X.L., He, Y.W., Fu, H.L. and Yin, Y.M. (2019), "Analytical analyses of the effect of filled karst cavern on tunnel lining structure under complex geological conditions", *AIP Adv.*, **9**(3). https://doi.org/10.1063/1.5079581.

Milad, Z., Masoud, R. and Daniel, D. (2020), "3D numerical investigation of segmental tunnels performance crossing a dip-slip fault", *Geomech. Eng.*, **23**(4): 351-364. https://doi.org/10.12989/gae.2020.23.4.351.

Muthulingam, S. and Rao, B.N. (2015), "Non-uniform corrosion states of rebar in concrete under chloride environment", *Corrosion Sci.*, **93**, 267-282. https://doi.org/10.1016/j.corsci.2015.01.031.

Qiu, P.Q., Wang, J., Ning, J.G., Liu, X.S., Hu, S.C. and Gu, Q.H. (2019), "Rock burst criteria of deep residual coal pillars in an underground coal mine: a case study", *Geomech. Eng.*, **19**(6), 499-511. https://doi.org/10.12989/gae.2019.19.6.499.

Song, L., Li, J.H., Garg, A. and Mei, G.X. (2018), "Experimental study on water exchange between crack and clay matrix", *Geomech. Eng.*, **14**(3), 283-291. https://doi.org/10.12989/gae.2018.14.3.283.

Vahab, S. and Abdollah, T. (2020), "Numerical simulation of the influence of interaction between Qanat and tunnel on the ground settlement", *Geomech. Eng.*, **23**(5), 455-466. https://doi.org/10.12989/gae.2020.23.5.455.

Wang, S.B. and Kang, Y.L. (2022), *Mechanics of Materials*, Higher Education Press, Bei Jing, China.

Wang, Q.S., Choe, K., Tang, J.Y., Shuai, C.J. and Wang, A.L. (2020), "Vibration analyses of general thin and moderately thick laminated composite curved beams with variable curvatures and general boundary conditions", *Mech. Adv. Mater. Struct.*, **27**(12), 991-1005. https://doi.org/10.1080/15376494.2018.1503760.

Wei, Y.K. (2021), "Application strategy of integrated geophysical prospecting in the treatment of a tunnel disease", *J. World Architect.*, **4**(6), 11-14. https://doi.org/10.26689/JWA.V4I6.1745.

Wen, S., Zhang, C.S. and Zhang, Y. (2019), "Favorable driving direction of double shield TBM in deep mixed rock strata: Numerical investigations to reduce shield entrapment", *Geomech. Eng.*, **17**(3), 237-245. https://doi.org/10.12989/gae.2019.17.3.237.

Zhou, W.F., Liao, S.M. and Men, Y.Q. (2021), "A fluid-solid coupled modeling on water seepage through gasketed joint of segmented tunnels", *Tunn. Undergr. Sp. Tech.*, 114, https://doi.org/10.1016/j.tust.2021.104008.

Zhuang, Y., Liu, X.R., Zhou, X.H. and Du, L.B. (2022), "Diffusion model of sulfate ions in concrete based on pore change of cement mortar and its application in mesoscopic numerical simulation", *Struct. Concrete*, **20**. https://doi.org/10.1002/suco.202100760.

IC